

## Nonconventional Phases of Colloidal Nanorods with a Soft Corona

Gerardo Campos-Villalobos,<sup>1,2,\*</sup> Marjolein Dijkstra,<sup>2</sup> and Alessandro Patti<sup>1,†</sup>

<sup>1</sup>*Department of Chemical Engineering and Analytical Science, University of Manchester, Sackville Street, Manchester M13 9PL, United Kingdom*

<sup>2</sup>*Soft Condensed Matter, Debye Institute for Nanomaterials Science, Department of Physics, Utrecht University, Princetonplein 1, 3584 CC Utrecht, The Netherlands*



(Received 26 October 2020; accepted 11 March 2021; published 12 April 2021)

Using computer simulations, we investigate the phase behavior of hard-core spherocylinders with a length-to-diameter ratio  $L/\sigma = 5$  and coated by a soft deformable corona of length  $\lambda/\sigma = 1.35$ . When quasi-two-dimensional layers are formed in smectic and solid phases at low temperatures, the competition between the two intrinsic length scales of the parallel aligned particles leads to the stabilization of different in-plane lattices of nonconventional symmetry, including low-density hexagonal, square, and high-density hexagonal crystals, as well as an intriguing dodecagonal quasicrystal. Our Letter opens up the opportunity to control the assembly of anisotropic nanoparticles into structures with preengineered symmetry-dependent physical properties.

DOI: [10.1103/PhysRevLett.126.158001](https://doi.org/10.1103/PhysRevLett.126.158001)

Prolate rodlike particles interacting via purely hard-core interactions show an especially rich phase behavior that is determined by particle shape anisotropy and system packing fraction [1–3]. In particular, rodlike particles can form isotropic (*I*) fluids, liquid crystalline nematic (*N*) and smectic (*SM*) phases, plastic crystals as well as orientationally ordered solids with “AAA” or “ABC” stacking. The unit cell of AAA- and ABC-stacked layers consists of parallel aligned rods forming packed structures with sixfold rotational symmetry. The inclusion of effective attractive forces (e.g., dispersion or depletion interactions) can induce nontrivial effects, such as the occurrence of a vapor-liquid critical point [4], a shift in the location of the liquid-crystal transition [5–7], and the apparent coexistence between more than two or three phases [8]. Nevertheless, these forces are not able to promote the formation of crystal phases with nonhexagonal symmetry. Since the early work of Hemmer and Stell [9], it has been recognized that hard-core spherically symmetric particles decorated by a soft-repulsive corona of variable shape can spark an especially complex phase behavior, where isostructural solid-solid transitions [10,11], liquid-liquid transitions [12], thermodynamic and dynamic anomalies [13–16], glass transitions [17], and the formation of various ordered structures in two and three dimensions [13,18,19] have been observed [20]. In the particular case of two-dimensional systems with double-scale isotropic repulsive interactions, the shape and energy and length scales of the potential soft-repulsive tail strongly influence the overall phase behavior and symmetry of the ordered structures [21–23], leading to interesting stripelike and honeycomb mesophases, labyrinths, Archimedean tilings, square lattices, and quasicrystals of different symmetry [24–29]. This rich morphology,

promoted solely by the incorporation of soft-repulsive interactions, has been recently observed experimentally in quasi-two-dimensional systems of polystyrene (PS) microspheres, coated with poly(*N*-isopropylacrylamide) microgels at the air-water interface [30], and monolayers of PS colloidal particles coated with polymeric amphiphiles [31].

Given the ability of hard spherocylinders of forming phases where particles are basically constrained in distinct two-dimensional layers [32–34], one may expect that adding a soft-repulsive shoulder would be sufficient to trigger the formation of nonhexagonal arrays of parallel rods, analogous to those found in strictly two-dimensional systems [27,35]. In suspensions of colloidal nanorods, Liang *et al.* reported the first experimental evidence of hexagonal symmetry breaking in mono- and multilayer superlattices of parallel aligned octagonal gold nanorods [36]. By modulating the effective interactions between the ligand-stabilized nanorods through surface functionalization, they observed a transition from high-density hexagonal to tetragonal molecular arrays, which exhibited an enhanced thermal stability and stronger plasmonic coupling. The authors concluded that this transition is governed entirely by an effective attractive interaction between pairs of standing rods. More recently, hexagonal-to-tetragonal transitions have been reported to take place in smectic phases of titanium oxide nanorods by controlling the grafting density of organic ligands [37]. In the latter case, the cores of the elongated particles were parallelepipeds with a square or rhombic cross section. Therefore, in addition to effective attractive interactions, the effect of the facets (core shape) on determining the symmetry of the packed structures cannot be easily ruled out.

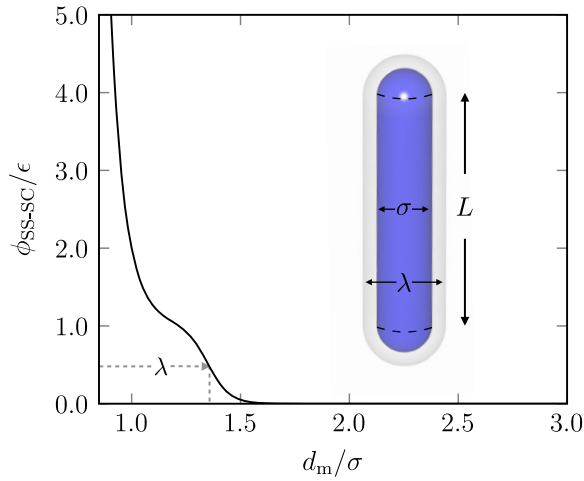


FIG. 1. SS-SC potential  $\phi_{\text{SS-SC}}(r, \Omega)$  as a function of the interparticle minimum distance  $d_m$  with  $k\sigma = 10$  and  $\lambda/\sigma = 1.35$ . Inset: a SS-SC with hard core of length-to-diameter ratio  $L/\sigma = 5$  and soft corona of thickness  $\sim(\lambda - \sigma)/2$ .

Inspired by these ideas, here we investigate the polymorphism in the equilibrium phases of spherocylindrical particles interacting via a double-scale purely repulsive potential. To demonstrate how soft-repulsive interactions between anisotropic particles can lead to a rich set of equilibrium phases beyond the conventional liquid-crystalline behavior, we consider elongated rods modeled as softened-square-shoulder spherocylinders (SS-SCs). The continuous pair potential for such a model can be written as

$$\phi_{\text{SS-SC}}(r, \Omega)/\epsilon = \left(\frac{\sigma}{d_m}\right)^{14} + \frac{1 - \tanh[k(d_m - \lambda)]}{2}, \quad (1)$$

where  $r$  and  $\Omega$  denote, respectively, the center-of-mass distance and relative orientation in space,  $d_m = d_m(r, \Omega)$  is the minimum distance between a pair of particles,  $\sigma$  is the hard-core diameter,  $\lambda$  is the characteristic length of the soft shoulder,  $\epsilon$  is the energy-scale parameter of the shoulder, and the constant  $k$  controls the steepness of the potential. This two-body potential for uniaxial rodlike particles is an extension of the Fermi-Jagla-like potential introduced by Ryzhov and co-workers [13], which has been widely employed to study the phase behavior of spherical particles in two and three dimensions [38]. Here, we investigate the phase behavior of a system of SS-SCs with a length-to-diameter ratio  $L^* \equiv L/\sigma = 5$  and shoulder length  $\lambda^* \equiv \lambda/\sigma = 1.35$ . The pair potential is characterized by  $k\sigma = 10$ , which was also used in previous studies on three- and two-dimensional fluids of spherically symmetric particles [13,27]. A pictorial representation of a SS-SC along with its pair potential is shown in Fig. 1

We study the phase behavior of SS-SCs by standard Metropolis Monte Carlo simulations in the isothermal-isobaric ensemble ( $NPT$ -MC) using rectangular simulation boxes with three-dimensional periodic boundary

conditions. In particular, we calculate the pressure-density equations of state (EOS) at reduced temperature  $0.12 \leq T^* \leq 0.30$  and reduced pressure  $0.05 \leq P^* \leq 10.0$ , with  $T^* \equiv k_B T/\epsilon$ ,  $P^* \equiv P\sigma^3/k_B T$ , and  $k_B$  as the Boltzmann constant. To this end, we expand systems of  $N = 1120$  particles initially arranged in a close-packed face-centered-cubic (fcc) lattice of four layers at  $\rho^* = N\sigma^3/V = 0.15$  [39]. Compression runs from low- to high-density states are also performed in the vicinity of phase transitions to check for hysteresis. To characterize the mesophases observed, we employ several global-order parameters. In particular, the degree of layering in the systems, indicating the occurrence of SM and crystal phases, is determined by measuring the smectic-order parameter, which reads

$$\tau = \max_d \left| \sum_{i=1}^N \exp\left(\frac{2\pi}{d} \mathbf{r}_i \cdot \hat{\mathbf{n}}\right) \right|, \quad (2)$$

where  $d$  is a real number related to the layer dimension,  $\mathbf{r}_i$  denotes the position of particle  $i$ , and  $\hat{\mathbf{n}}$  is the nematic director. Additionally, the two-dimensional bond-order parameters,  $\Psi_4$ ,  $\Psi_6$ , and  $\Psi_{12}$  are calculated to identify 4-, 6-, and 12-fold bond angular order, respectively, in the discrete layers of SM and crystalline phases. More specifically,

$$\Psi_n = \left\langle \frac{1}{N_l} \left| \sum_{j=1}^{N_l} \frac{1}{N_j} \sum_{m=1}^{N_j} \exp(in\theta_{jm}) \right| \right\rangle_l, \quad (3)$$

where  $n$  is the symmetry of interest,  $N_l$  is the number of particles in layer  $l$ ,  $N_j$  is the number of nearest neighbors around particle  $j$  [40],  $\theta_{jm}$  is the angle between the center-of-mass distance vector between particles  $j$  and  $m$ , and an arbitrary reference axis in the plane of layer  $l$  (with normal  $\hat{\mathbf{n}}$ ), and the brackets  $\langle \dots \rangle_l$  denote an ensemble average over the layers. To fully characterize the phase symmetry, in-layer structure factors and two-dimensional pair-correlation functions,  $g_{\perp,l}(r)$  perpendicular to the main director, are also calculated.

The temperature-density ( $T^* - \rho^*$ ) phase diagram is reported in Fig. 2, whereas isotherms of the EOS and order parameters are reported in the Supplemental Material [41] (also see [42]). Overall, we detect the formation of seven different stable phases in the studied parameter space: isotropic fluids  $I$ , with nearly vanishing values of  $\tau$  and no long-ranged orientational correlations; smectic phases with  $\tau \sim 1$  and no overlap (SM\*) or partial overlap (SM) between the particle coronas; low-density hexagonal, high-density hexagonal, and square solid phases; and, remarkably, dodecagonal quasicrystal phases. In the LDH, HDH, and SQ solid phases, ordered adjacent layers display the typical  $ABC$  fcc stacking. The isostructural LDH and HDH solids display different lattice spacings between the in-layer rods. While in the LDH phase, parallel

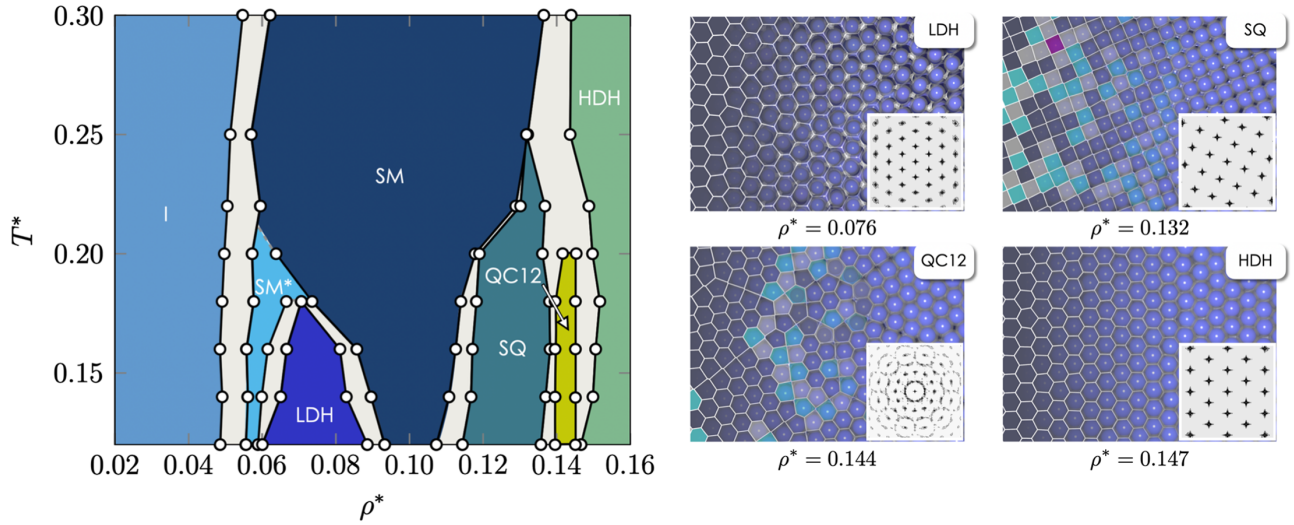


FIG. 2. Left: phase diagram of a system of SS-SCs of shoulder length  $\lambda/\sigma = 1.35$  in the temperature  $T^* = k_B T/\epsilon$ -density  $\rho^* = N\sigma^3/V$  plane with  $N$  as the number of particles and  $V$  as the volume of the system. Labels indicate isotropic  $I$  fluids; smectic liquid crystals with (SM) or without (SM\*) overlap between particle coronas; square (SQ), low-density hexagonal (LDH) and high-density hexagonal (HDH) crystals; and dodecagonal quasicrystals (QC12). Gray-shaded areas indicate the coexistence regions. Right: representative simulation snapshots (top view) showing the in-layer arrangement of LDH, SQ, QC12, and HDH phases formed by SS-SCs at  $T^* = 0.12$ . The corresponding structure factors and Voronoi tessellations are also included. The coloring scheme of the particles is the same as in Fig. 1.

aligned rods organize into hexagonal arrays in order to avoid overlap of their shoulder  $\lambda$ , in the HDH solid, the shoulders fully overlap and the rods are at close contact at a distance corresponding to the hard-core diameter  $\sigma$ . Simulation snapshots and structure factors, showing the typical ordering of the parallel aligned rods in the quasi-two-dimensional layers are illustrated in Fig. 2.

In light of these preliminary observations, we now discuss the conditions driving the formation of the phases shown in Fig. 2. At the highest temperature ( $T^* = 0.30$ ), the system is found in a typical  $I$  phase for densities  $\rho^* < 0.054$ . Upon increasing density, the system exhibits a first-order  $I$ -SM phase transition as suggested by the steep increase in the smectic-order parameter, which equals  $\tau = 0.854$  at  $\rho^* = 0.062$ . First-order  $I$ -SM transitions are also observed in systems of hard spherocylinders (HSCs) with length-to-diameter ratio  $3.1 < L^* < 3.7$  [3]. For larger values of  $L^*$ , the  $I$ -SM transition in HSCs is preempted by the  $N$  phase. While the SS-SC fluid becomes nearly equivalent to the HSC fluid with  $L^* = 5$  in the high-temperature limit, at the finite temperatures explored here and at low densities, it can be regarded as being composed of HSCs with an effective length-to-diameter ratio  $L_{\text{eff}}^* = L/\lambda \sim 3.7$  [43]. Such a smaller aspect ratio, as also observed for HSCs, inhibits the formation of  $N$  phases, while promoting a direct  $I$ -SM transition. The resulting SM phase is stable in a wide range of densities ( $0.062 < \rho^* \leq 0.136$ ) due to the interplay between the two relevant length scales of the pair potential, which permits compression without any phase transformation. The existence of these two competing length scales is

evidenced by the in-layer pair-correlation function  $g_{\perp,l}(r)$  reported in Fig. 3. In particular, the pronounced second peak of  $g_{\perp,l}(r)$  in the low-density SM phase suggests that particles are preferentially found at relative distances slightly larger than  $\lambda$ , where their soft shoulders are in close contact to each other. However, at such low densities, close contact between hard cores is also observed as indicated by the first peak of  $g_{\perp,l}(r)$ . At larger densities, the second peak in  $g_{\perp,l}(r)$  becomes irrelevant with respect to the first peak, indicating a high degree of overlap between the particle coronas. The layers of low-density

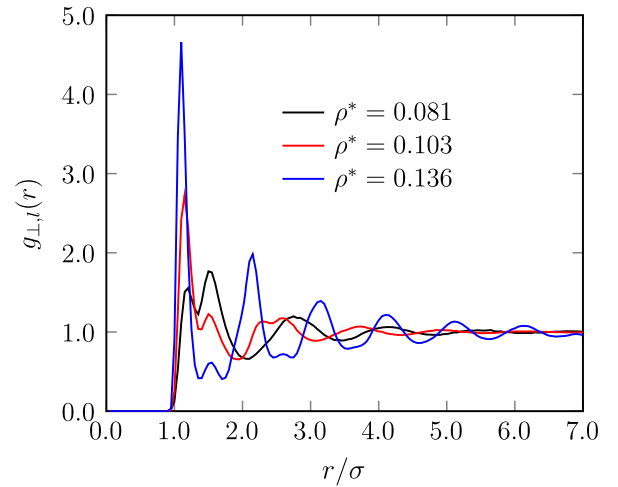


FIG. 3. Two-dimensional (in-layer) pair-correlation function  $g_{\perp,l}(r)$  of SS-SCs as a function of distance  $r$  in the SM phases at temperature  $T^* = 0.30$  and varying density  $\rho^*$  as labeled.

SM phases can therefore be regarded as pseudobinary mixtures of rodlike particles of diameter  $\sigma$  and of diameter  $\lambda$ . Upon increasing pressure, the prevailing characteristic length  $\sigma$  ultimately leads to the extinction of the latter set of particles and to a first-order SM-HDH phase transition observed at  $\rho^* = 0.136\text{--}0.143$ .

At temperature  $T^* = 0.25$ , an  $I$ -SM transition is observed at  $\rho^* = 0.051\text{--}0.057$ . In this case, the SM phase is stable up to  $\rho^* = 0.130$ , where a smooth transition to a crystal phase is detected. Interestingly, in this solid phase, the large value of  $\Psi_4$  confirms that particles in the same layer arrange into a square lattice (SQ phase). The subsequent transformation of the SQ to the HDH phase at this temperature occurs at  $\rho^* = 0.131\text{--}0.143$ . At temperature  $T^* = 0.22$ , a similar sequence is observed and the SQ phase becomes stable in a relatively wider range of densities. When the system is at  $T^* = 0.20$ , the  $I$  phase transitions into a smectic  $SM^*$  phase upon increasing density. We differentiate this phase from the typical SM phase based on the in-layer arrangement of particles. As discussed above, both phases present unidimensional translational order along the director (large  $\tau$  values) and exhibit in-plane fluidlike structure (vanishing  $\Psi_n$  values). However, in the  $SM^*$  phase, no overlaps between the particles' coronas occur, while in the SM phase, a large degree of overlap is detected. Such a difference can be appreciated in the pair-correlation functions (Supplemental Material [41]) and is ultimately due to the increased energetic penalty associated with shoulder overlap at low temperatures. Since this transition only involves the continuous compression of particles without significant symmetry rearrangement, no density jumps are detected and, therefore, no coexistence occurs. By further compressing the SM phase, a SQ crystal that spans the range of densities  $0.119 \leq \rho^* \leq 0.136$  is formed. As the SM-SQ transition is closely related to the freezing of the quasi-two-dimensional liquid layers, it is relevant to compare the density at which this transition occurs with the analogous freezing density of softened-square-shoulder disks. At  $T^* = 0.20$ , the quasi-two-dimensional in-layer densities of the coexisting SM and SQ phases are  $\rho_{2D,SM}^* = 0.772$  and  $\rho_{2D,SQ}^* = 0.796$ , respectively. In two-dimensional systems of softened-square-shoulder disks, the transition from liquidlike to square lattices, at the same temperature, occurs at  $\rho_{2D}^* \sim 0.8$  [27,35,44].

It is important to mention that one of the most interesting features of two-dimensional square-shoulder disks is their apparent ability to form dodecagonal quasicrystals, which have been typically found in between square and high-density hexagonal phases at  $0 < T^* < 0.3$  [21,27,35]. For the particular case of softened-square-shoulder disks, with similar potential parameters to those employed in our MC simulations, the stability of such an intriguing quasicrystal is limited to a rather narrow portion of the phase diagram, covering only the approximate range  $0.92 < \rho_{2D}^* < 0.95$ . Interestingly, for the three-dimensional anisotropic SS-SCs,

we detect stable layered phases exhibiting a marked 12-fold rotational symmetry for temperatures  $T^* < 0.20$  and densities intermediate between the SQ and HDH crystals. As in the case of two-dimensional systems [21], we obtain such QC12 phases by MC- $NVT$  simulations, where HDH crystals are cooled from a high to a low temperature ( $T^* = 1.0$  to  $0.12$ ), keeping the quasi-2D density in the range  $0.92 < \rho_{2D,QC12}^* < 0.95$  [45]. Dodecagonal quasicrystals have been also observed in three-dimensional systems of particles interacting through different isotropic potentials [46–48], as well as in purely hard polyhedra [49,50]. The ability of SS-SCs to form QC12 phases makes them the first exemplary case of prolate spherocylindrical particles able to form soft-matter dodecagonal quasicrystals.

The dual-scale character of SS-SCs becomes more evident at lower temperatures, sparking the stability of another phase. In particular, we observe that, at  $T^* = 0.18$ , the continuous  $SM^*$ -SM transition is inhibited. Instead, due to the increasing energy penalty associated with the overlap of the particle coronas, a LDH phase is found immediately after compressing the  $SM^*$  phase. The analogous transition between an isotropic fluid and a low-density hexagonal lattice occurs in 2D systems at  $\rho_{2D}^* \sim 0.45$  [35], whereas the quasi-two-dimensional in-layer density at which the LDH is formed in our system is  $\rho_{2D,LDH}^* = 0.467$ . This atypical low-density solid phase, eventually *melts* as a result of the partial overlap between the particle coronas when the density is increased. The resulting SM phase is bounded at  $\rho^* > 0.117$  by a SQ phase, which eventually transitions into a QC12 at  $\rho^* \geq 0.138$ , and finally into a HDH solid at  $\rho^* \geq 0.145$ . The quasi-2D density at which the HDH appears in this case corresponds to  $\rho_{2D,HDH}^* = 0.997$ , which is again in partial quantitative agreement with the 2D system, where the transition from a dodecagonal quasicrystal to a high-density hexagonal lattice takes place at  $\rho_{2D}^* \sim 0.99$  [35]. In the range of temperatures  $0.12 \leq T^* \leq 0.16$ , all seven phases are stable. In particular, we observe that, as the regions for the LDH and SQ phases widen, the SM and  $SM^*$  phases with fluidlike in-layer structure occupy a narrower range of densities. In spherically symmetric particles with double-scale isotropic interactions, glass transitions have already been reported [17]. Investigating the dynamics of the SS-SC fluid and resolving whether these anisotropic particles can lead to the formation of orientational glasses is left as a future task.

Finally, in order to verify whether an  $N$  phase is stable in the SS-SC system, the isotherm of the EOS of a system of  $N = 1600$  SS-SCs with  $L/\sigma = 10$  (effective  $L/\lambda \sim 7.4$ ) is computed at  $T^* = 0.12$  (Supplemental Material [41]). We find that upon increasing density, an  $I - N$  transition precedes the transformation into the layered states presenting distinct in-layer symmetries as observed in systems with  $L/\sigma = 5$ . Interestingly, the range of packing fractions where this  $N$  phase is stable matches the case of HSCs with  $L/D = 7.4$ . The effect of the energy and length scale of the

pair potential, as well as particle shape anisotropy on the phase behavior of SS-SC particles, will be the subject of a work currently in preparation.

In summary, our MC simulations evidence the non-conventional phases that can be stabilized in SS-SC systems by the interplay of particle shape anisotropy, which determines the liquid crystalline phase behavior and the competition between the two length scales of the purely repulsive pair potential, which can stabilize quasi-two-dimensional layers with distinct complex symmetry. In particular, at the studied temperatures and at low densities, the SS-SCs display the features of HSCs with an approximate effective length-to-diameter  $L/\lambda$ . When layered phases form, the reversible transitions detected between different in-plane lattices closely fit into the phase behavior of truly two-dimensional softened-square-shoulder disks [27,35]. Interestingly, our results suggest that nonhexagonal assemblies of standing aligned colloidal rods can be realized by purely repulsive interactions and not necessarily by the introduction of effective highly nonmonotonic attractive interactions as recently suggested [36]. The observations discussed herein may open up a new way for controlling the assembly of anisotropic nanoparticles into structures with symmetry-dependent mechanical, optical, and electrical properties demanded in optoelectronic devices, enhanced spectroscopies, and solar cells [51].

G. C. V. acknowledges Carlos Avendaño (University of Manchester) for stimulating discussions. The project leading to these results has received funding from the European Union Horizon 2020 Research and Innovation Programme under the Marie Skłodowska-Curie Grant No. 676045 (MULTIMAT).

\*g.d.j.camposvillalobos@uu.nl

†alessandro.patti@manchester.ac.uk

- [1] D. Frenkel, H. Lekkerkerker, and A. Stroobants, *Nature (London)* **332**, 822 (1988).
- [2] J. A. C. Veerman and D. Frenkel, *Phys. Rev. A* **41**, 3237 (1990).
- [3] P. Bolhuis and D. Frenkel, *J. Chem. Phys.* **106**, 666 (1997).
- [4] B. Martínez-Haya, L. Rull, A. Cuetos, and S. Lago, *Mol. Phys.* **99**, 509 (2001).
- [5] D. C. Williamson and F. del Rio, *J. Chem. Phys.* **109**, 4675 (1998).
- [6] A. Gil-Villegas, S. C. McGrother, and G. Jackson, *Chem. Phys. Lett.* **269**, 441 (1997).
- [7] S. C. McGrother, A. Gil-Villegas, and G. Jackson, *Mol. Phys.* **95**, 657 (1998).
- [8] V. F. D. Peters, M. Vis, Á. G. García, H. H. Wensink, and R. Tuinier, *Phys. Rev. Lett.* **125**, 127803 (2020).
- [9] P. Hemmer and G. Stell, *Phys. Rev. Lett.* **24**, 1284 (1970).
- [10] P. Bolhuis and D. Frenkel, *J. Phys. Condens. Matter* **9**, 381 (1997).
- [11] A. Denton and H. Löwen, *J. Phys. Condens. Matter* **9**, L1 (1997).
- [12] Y. D. Fomin, V. N. Ryzhov, and E. E. Tareyeva, *Phys. Rev. E* **74**, 041201 (2006).
- [13] Y. D. Fomin, N. Gribova, V. Ryzhov, S. Stishov, and D. Frenkel, *J. Chem. Phys.* **129**, 064512 (2008).
- [14] N. V. Gribova, Y. D. Fomin, D. Frenkel, and V. N. Ryzhov, *Phys. Rev. E* **79**, 051202 (2009).
- [15] Y. D. Fomin, V. N. Ryzhov, and N. V. Gribova, *Phys. Rev. E* **81**, 061201 (2010).
- [16] Y. D. Fomin, E. Tsiok, and V. Ryzhov, *J. Chem. Phys.* **135**, 234502 (2011).
- [17] G. Das, N. Gnan, F. Sciortino, and E. Zaccarelli, *J. Chem. Phys.* **138**, 134501 (2013).
- [18] G. Malescio and G. Pellicane, *Nat. Mater.* **2**, 97 (2003).
- [19] H. Pattabhiraman, G. Avvisati, and M. Dijkstra, *Phys. Rev. Lett.* **119**, 157401 (2017).
- [20] S. B. Yuste, A. Santos, and M. López de Haro, *Mol. Phys.* **109**, 987 (2011).
- [21] H. Pattabhiraman and M. Dijkstra, *J. Phys. Condens. Matter* **29**, 094003 (2017).
- [22] E. Jagla, *Phys. Rev. E* **58**, 1478 (1998).
- [23] E. Jagla, *J. Chem. Phys.* **110**, 451 (1999).
- [24] H. Pattabhiraman and M. Dijkstra, *Soft Matter* **13**, 4418 (2017).
- [25] H. Pattabhiraman and M. Dijkstra, *J. Chem. Phys.* **146**, 114901 (2017).
- [26] H. Pattabhiraman, A. P. Gantapara, and M. Dijkstra, *J. Chem. Phys.* **143**, 164905 (2015).
- [27] N. P. Kryuchkov, S. O. Yurchenko, Y. D. Fomin, E. N. Tsiok, and V. N. Ryzhov, *Soft Matter* **14**, 2152 (2018).
- [28] T. Dotera, T. Oshiro, and P. Ziherl, *Nature (London)* **506**, 208 (2014).
- [29] H. G. Schoberth, H. Emmerich, M. Holzinger, M. Dulle, S. Förster, and T. Gruhn, *Soft Matter* **12**, 7644 (2016).
- [30] M. Rey, A. D. Law, D. M. A. Buzza, and N. Vogel, *J. Am. Chem. Soc.* **139**, 17464 (2017).
- [31] M. Rey, T. Yu, K. Bley, K. Landfester, D. M. A. Buzza, and N. Vogel, *Langmuir* **34**, 9990 (2018).
- [32] E. Grelet, M. P. Lettinga, M. Bier, R. Van Roij, and P. Van der Schoot, *J. Phys. Condens. Matter* **20**, 494213 (2008).
- [33] A. Patti, D. El Masri, R. van Roij, and M. Dijkstra, *Phys. Rev. Lett.* **103**, 248304 (2009).
- [34] A. Patti and A. Cuetos, *Phys. Rev. E* **86**, 011403 (2012).
- [35] L. A. Padilla and A. Ramírez-Hernández, *J. Phys. Condens. Matter* **32**, 275103 (2020).
- [36] Y. Liang, Y. Xie, D. Chen, C. Guo, S. Hou, T. Wen, F. Yang, K. Deng, X. Wu, I. I. Smalyukh *et al.*, *Nat. Commun.* **8**, 1410 (2017).
- [37] S. N. Hosseini, A. Grau-Carbonell, A. G. Nikolaenkova, X. Xie, X. Chen, A. Imhof, A. van Blaaderen, and P. J. Baesjou, *Adv. Funct. Mater.* **30**, 2005491 (2020).
- [38] See Ref. [27] and citations therein.
- [39] Expansion runs consist of up to  $10^7$  MC cycles, where a cycle corresponds to  $N$  attempts of rotating and/or translating particles plus one volume move.
- [40] For  $\Psi_{12}$  and  $\Psi_6$ ,  $N_j$  is calculated using the Voronoi tessellation, while for  $\Psi_4$ , the four closest neighbors of each particle are used.
- [41] See Supplemental Material at <http://link.aps.org/supplemental/10.1103/PhysRevLett.126.158001> for a description of the isotherms of the equations of state of

- SS-SCs with  $L/\sigma = 5$  and 10, details on the characterization of smectic phases and on MC simulations of QC12 phases.
- [42] We note that phase transition densities as obtained from expansion and compression runs differ by at most  $|\rho_{\text{compression}}^* - \rho_{\text{expansion}}^*| = 0.005$ .
- [43] Since the particle shoulder extends beyond the exact value of  $\lambda$  (Fig. 1),  $L_{\text{eff}}^*$  is slightly smaller than 3.7.
- [44] D. Dudalov, Y. D. Fomin, E. Tsiok, and V. Ryzhov, *J. Phys. Conf. Ser.* **510**, 012016 (2014).
- [45] To prove the stability of such phases, additional simulations are performed using a configuration consisting of smectic layers having the parallel aligned rods in dodecagonal motifs arranged in a triangle tiling.
- [46] X. Ye, J. Chen, M. E. Irrgang, M. Engel, A. Dong, S. C. Glotzer, and C. B. Murray, *Nat. Mater.* **16**, 214 (2017).
- [47] P. F. Damasceno, S. C. Glotzer, and M. Engel, *J. Phys. Condens. Matter* **29**, 234005 (2017).
- [48] A. Metere, P. Oleynikov, M. Dzugutov, and S. Lidin, *Soft Matter* **12**, 8869 (2016).
- [49] A. Haji-Akbari, M. Engel, A. S. Keys, X. Zheng, R. G. Petschek, P. Palfy-Muhoray, and S. C. Glotzer, *Nature (London)* **462**, 773 (2009).
- [50] A. Haji-Akbari, M. Engel, and S. C. Glotzer, *Phys. Rev. Lett.* **107**, 215702 (2011).
- [51] P. Li, Y. Li, Z.-K. Zhou, S. Tang, X.-F. Yu, S. Xiao, Z. Wu, Q. Xiao, Y. Zhao, H. Wang *et al.*, *Adv. Mater.* **28**, 2511 (2016).